Chemical Engineering Science 104 (2013) 319–329

Contents lists available at ScienceDirect

Chemical Engineering Science

journal homepage: www.elsevier.com/locate/ces

Granule size distribution for a multi-chamber fluidized-bed melt granulator: Modeling and validation using process measurement data

Diego E. Bertin *, Ivana Cotabarren, Juliana Piña, Verónica Bucalá

Department of Chemical Engineering – Universidad Nacional del Sur (UNS), Planta Piloto de Ingeniería Química (PLAPIQUI) – UNS-CONICET, Camino La Carrindanga Km. 7, 8000 Bahía Blanca, Argentina

HIGHLIGHTS

- We model a multi-chamber fluidized-bed granulator used for urea production.
- The model has mass, energy and population balances for all the fluidized beds.
- The model including coating and elutriation is consistent with industrial data.
- A method is proposed to reduce the errors in the population balance solution.
- The fines are removed almost completely in the first and second chambers.

ARTICLE INFO

Article history:
Received 24 April 2013
Received in revised form
15 July 2013
Accepted 8 August 2013
Available online 23 August 2013

Keywords:
Melt granulation
Industrial fluidized-bed
Population balance equation
Elutriation

ABSTRACT

In this work, a steady-state model of a multi-chamber fluidized-bed granulator used for urea production is developed and validated. To this aim, mass, energy and population balances are solved for all the fluidized beds. Regarding the population balance equation (PBE), pure coating or the combined mechanisms of coating and elutriation are taken into account. Both PBE formulations are analytically solved and a new solution methodology is proposed to handle inlet solid streams distributed in different size grids and to minimize the solution errors propagation expected when a set of PBEs in series has to be solved. By comparison with experimental data, it is found that the model including coating and elutriation gives a better representation of the particles size distribution with respect to the results found when pure coating is assumed. Besides, the results indicate that the fines are removed almost completely in the first and second chambers, being the amount of fines in the subsequent chambers negligible.

1. Introduction

Flowsheet simulation of industrial processes has nowadays become essential to take advantage of new and cost effective software tools for plant design, troubleshooting, control strategies improvements, optimization, workforce education, etc. (Dosta et al., 2010; Reimers et al., 2009). Therefore, there is need to develop modern simulation packages capable to integrate accurate equipment models. In large-scale plants, reliable simulators can help to identify optimal operating conditions that allow increasing industries benefits significantly (Werther et al., 2011).

Although 60% of industrial chemical products are particulate in nature and a further 20% use powder intermediates (Ennis, 1997), simulation tools for plants that handle particulate systems are not as well developed as those for liquid/gas based industries. The modeling of processes involving powders or granules is difficult because, among other reasons, they have to be described as distributed systems. Consequently, the mathematical representation of powders transformations is not a trivial task. In fact, these models called population balance equations (PBE) are described by a set of complex partial integro-differential equations (Dosta et al., 2010; Reimers et al., 2009; Werther et al., 2011).

Within the operations that handle solids, granulation is considered as one of the most important advances. It is a key particle size enlargement process, widely used in the pharmaceutical, food, mining and fertilizer industries, which converts fine particles and/or atomizable liquids (suspensions, solutions, or melts) into granular material with desired properties (Adetayo et al., 1995; Tan et al., 2006). Even though granulation is accepted as an overwhelming particle size enlargement unit operation, not all the particles that leave the granulator meet the marketable granules size distributions. To this end, other unit operations are necessary (such as crushing and size classification stages). Therefore, the granulator along with

* Corresponding author. Tel: +54 291 486 1700x268; fax: +54 291 486 1600.
E-mail addresses: dbertin@plapiqui.edu.ar, diegobertin@yahoo.com (D.E. Bertin).

0009-2509/$ - see front matter © 2013 Elsevier Ltd. All rights reserved.
http://dx.doi.org/10.1016/j.ces.2013.08.012

crushers and screens constitute the granulation circuit. The operation of granulation circuits is not simple and often presents operational challenges, which force them to work with a capacity less than the nominal one and with high recycle ratios that overload all process units (Balliu, 2005; Cotabarren et al., 2011; Wang and Cameron, 2007). In particular, the recycle characteristics greatly influence the granulation unit operation. This stream represents a continuous feedback of mass, energy and a certain particle size distribution to the granulator, producing frequent oscillations in the process variables. Depending on the operating conditions, these oscillations are damped or generate increasing instabilities that may cause undesired plant shutdowns. The oscillations, in turn, lead to a granular product with properties that vary in time (Radichkov et al., 2006). In view of the operational complexity associated to processes that handle particulate systems, research related to process modeling for the development of robust simulators applied to the solids industry has been intense in recent years (Adetayo, 1993; Balliu and Cameron, 2007; Dosta et al., 2010; Gatzke and Doyle, 2001; Sanders et al., 2009; Werther et al., 2011; Wildeboer, 1998).

Granulation circuit models can be used with confidence to address key design changes only if they are validated against collected data (Balliu and Cameron, 2007). Particularly, the modeling of large-scale industrial granulators requires identifying the main size change mechanisms and consequently formulating and accurately solving the PBE, and finally fitting the corresponding kinetic parameters by taking into account experimental data.

In this context, this article is focused on the mathematical model development and validation of a multi-chamber fluidized-bed melt granulator used for urea production. This particular process has been selected as an interesting case of study because there are many large-scale urea plants around the world operating with fluidized-bed granulation technologies as finishing process (Cotabarren et al., 2012), which require validated simulators to improve process performance and, thus, plant profitability. The main goal of this work is to provide a steady-state model of a multi-chamber fluidized-bed granulator, accurate enough to be reliably applied in industry for process simulation, optimization and control purposes. To this aim, pure coating and the combined mechanisms of coating and elutriation were proposed. The different PBE formulations were analytically solved and a new solution methodology was proposed to handle inlet solid streams distributed in different size grids and to minimize the solution errors propagation expected when a set of PBEs in series is required to be solved. Finally, based on data collected from a large-scale urea plant, a kinetic parameter are given.

2. Description of the multi-chamber fluidized-bed melt granulator

Although urea granulation can be performed in different types of granulators, fluidized-bed units are commonly used for large-scale production due to their versatility and potential to carry out the process at low costs (Mörl et al., 2007). Fig. 1 presents a simplified schematic representation of the urea fluidized-bed granulator. This unit is basically a bed of solids fluidized by air, continuously fed with small urea particles (called seeds) and a urea highly concentrated liquid solution (about 96%) that is sprayed from the bottom (Niks et al., 1980). The bubbling nature of the fluidized bed, which is responsible for the strong solids mixing, promotes the repeatedly circulation of the granules through the spray zone. The unit is designed and operated with the purpose of favoring granules growth through a coating process, which consists in the deposition of tiny liquid droplets onto the seeds followed by cooling and water evaporation that facilitate the solidification of the sprayed urea. The energy for evaporation is provided by the urea solution itself, which is atomized into the granulator at a relatively high temperature (Bertin et al., 2007). In order to increase the granules residence time and to reduce the dispersion of the outlet particle size distribution (PSD), industrial granulators have several growth chambers (where the urea concentrated solution is sprayed) connected through the bottom of the unit. Subsequently, fluidized-bed dedusting/cooling compartments are arranged to meet specific requirements for further granules processing. In particular, Fig. 1 shows a typical configuration of an industrial urea granulator, constituted by 3 growth chambers and 3 cooling ones.

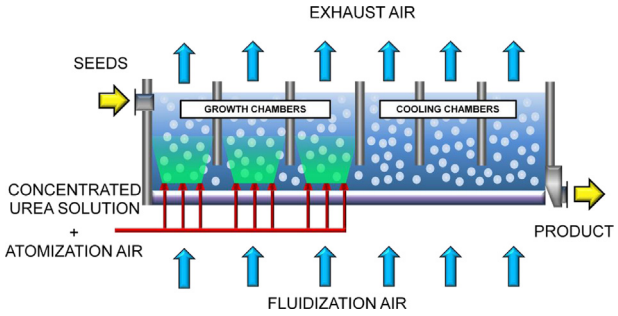

Fig. 1. Schematic representation of a multi-chamber fluidized-bed granulator for urea production.

Even though coating is the preferred growth mechanism, unexpected operating conditions may favor undesired particles size change phenomena. Therefore, it is necessary to identify the main size change mechanisms that may take place within the unit.

3. Fluidized-bed granulator model: pure coating growth

The starting model for the urea fluidized-bed granulator is founded on the assumptions of pure coating growth and a coating efficiency of 100% (i.e., all the urea present in the atomized solution successfully contributes to particles growth).

3.1. Mathematical model

Considering the unit features above described (Fig. 1) and previous simulation results on the steady and unsteady-state operations of the multi-chamber granulator (Bertin et al. 2007, 2010, 2011), the steady-state model of the industrial fluidized-bed urea granulator is formulated on the basis of the following hypotheses:

- The solid phase is perfectly mixed within the fluidized beds. As it is known, the degree of mixing within the granulator has an important effect on the granule size distribution. It has been observed that the experimental PSD greatly broadens along the granulator chambers (from the inlet to the outlet). Moreover, it has been found that the exponential residence time distribution of the particles provided by the assumption of perfect mixing in each fluidized growth chamber was enough to achieve consistency between the real and simulated PSDs.
- In each chamber, all the urea granules have the same density and porosity and are spherical.
- All the urea melt droplets successfully reach the solids surface and contribute to the particles growth (i.e., perfect coating efficiency). The sprayed droplets are distributed proportionally to the fraction of total particles surface area (Litster et al., 2004; Mörl et al., 2007).
- Coating is the only size change mechanism, i.e. the elutriation of fines, formation of nuclei by attrition, agglomeration, breakage and overspray are negligible.

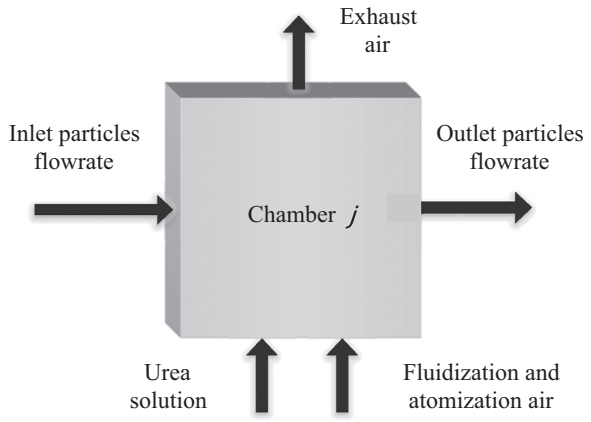

Fig. 2. Scheme of a granulation chamber showing the main streams and variables.

- The urea seeds are virtually dry (Kayaert and Antonus 1997).
- The water content of the urea melt droplets is instantaneously and completely evaporated (Bertin et al., 2007).
- Due to the intense mixing provided by the fluidization, the air and solid temperatures within each chamber are equal (Bertin et al., 2007).
- The product discharge is non-classified.

Fig. 2 shows, for a growth chamber, the main streams and nomenclature used to denote mass and number flowrates and water content in the urea solution.

3.1.1. Mass balances

The steady-state urea mass balance for a chamber j (see Fig. 2) is given by

$$\dot{m}^j_{S_{in}} + \dot{m}^j_L(1-x^j_L) - \dot{m}^j_{S_{out}} = 0 \quad j = 1\text{–}6 \tag{1}$$

where $\dot{m}^j_{S_{in}}$ and $\dot{m}^j_{S_{out}}$ are the inlet and outlet particles mass flowrates, respectively. Due to the series configuration of the chambers, for $j=2$–6 $\dot{m}^j_{S_{in}} = \dot{m}^{j-1}_{S_{out}}$. $\dot{m}^j_L$ and x^j_L represent the urea solution mass flowrate atomized into chamber j and its water mass fraction, respectively. Considering that the granulator has three growth chambers (1–3) and three cooling compartments (4–6), $\dot{m}^j_L = 0$ for chambers 4–6.

3.1.1.1. Outlet mass flowrates and fluidized-bed heights. The urea particles flow in the horizontal direction, from the first to the last chamber, driven by the pressure drop between compartments (Grieco and Marmo, 2006; Massimilla et al., 1961). By means of the Bernoulli equation, the kinetic energy of the particles flowing from one chamber to another is related to the pressure difference between chambers

$$\frac{1}{2}\rho^j_{bed}\left(\frac{\dot{m}^j_{S_{out}}}{\rho^j_{bed}A^j_0}\right)^2 = \rho^j_{bed} g L^j - \rho^{j+1}_{bed} g L^{j+1} \quad j = 1\text{–}5 \tag{2}$$

where g is the gravity acceleration, A^j_0 the passage area between chambers, ρ^j_{bed} the bed density, and L^j the fluidized-bed height. Solving the equation for $\dot{m}^j_{S_{out}}$

$$\dot{m}^j_{S_{out}} = C_D\, A^j_0 \sqrt{2g\,\rho^j_{bed}\,(\rho^j_{bed}\,L^j - \rho^{j+1}_{bed}\,L^{j+1})} \quad j = 1\text{–}5 \tag{3}$$

where C_D, the discharge coefficient, has been included and set at 0.5, as suggested by Massimilla (1971) for particles much smaller than the passage or discharge areas.

Similarly, the particles discharge through the granulator outlet is expressed by the following equation:

$$\dot{m}^6_{S_{out}} = C_D\,\rho^6_{bed} A^6_0 \sqrt{2gL^6} \tag{4}$$

where A^6_0 is the discharge area of the last chamber.

Eqs. (3) and (4) are used to calculate the fluidized-bed heights, considering the particles mass flowrates obtained from Eq. (1).

3.1.1.2. Fluidized-bed densities and porosities. The fluidized-bed density for each chamber j is defined as

$$\rho^j_{bed} = \rho_p(1-\varepsilon^j) + \rho^j_a\,\varepsilon^j \tag{5}$$

Being ρ_p and ρ^j_a the particle and fluidization air densities, respectively. According to Mörl et al. (2007), the fluidized-bed porosity (ε^j) is estimated through the correlation given by Richardson and Zaki (1954). The bed porosity is a function of the air superficial velocity, the Sauter mean diameter of the particles population and physical properties of the solids and gas.

Once the fluidized-bed porosity is known, the particles mass within each chamber can be calculated as $m^j_S = \rho_p(1-\varepsilon^j)A^j_T L^j$, where A^j_T is the cross-sectional area of chamber j.

3.1.2. Energy balances

Different thermal effects take place in the urea granulator. In addition to the sensible heats associated to the inlet and outlet streams, latent heats (urea dissolution and water evaporation) are involved in the growth chamber energy balances. Considering the assumptions above discussed, the steady-state energy balance for the granulator (which has been validated against plant data) is given by Bertin et al. (2011).

3.1.3. Population balance equation

Considering the particles size Dp as the internal coordinate, that only pure coating growth takes place and each granulator compartment behaves as a well-mixed system, the steady-state PBE for the granulator chamber j becomes (Ramkrishna, 2000)

$$\frac{d}{dDp}(G^j n^j) = \dot{n}^j_{in} - \dot{n}^j_{out} \quad j = 1\text{–}6 \tag{6}$$

where G^j is the coating growth rate and $\dot{n}^j_{in}$ and $\dot{n}^j_{out}$ are the density function flowrates associated to the particles entering and leaving each chamber, respectively. The growth rate G^j, which describes the deposition of small urea droplets onto the particles surface, is defined as the material derivative of the particle size. Then, according to the first three assumptions given in Section 3.1, G^j becomes (Litster et al., 2004)

$$G^j = \frac{dDp}{dt} = \frac{2\dot{m}^j_L\,(1-x^j_L)}{\rho_p\,Ap^j_T} \tag{7}$$

where Ap^j_T denotes the total particles surface area within chamber j. This equation states that all the particles, independently of their sizes, grow at the same rate (i.e., G^j is not a function of Dp). Considering that $\tau^j = m^j_S/\dot{m}^j_{S_{out}}$ (where m^j_S is the mass of solids within chamber j), τ^j represents the mass mean residence time of the particles in chamber j. If the solids are perfectly mixed, the relationship $\dot{n}^j_{out} = n^j/\tau^j$ is verified. Therefore, Eq. (6) can also be written as

$$G^j\frac{dn^j}{dDp} = \dot{n}^j_{in} - \frac{n^j}{\tau^j} \tag{8}$$

The steady-state PBE given by Eq. (8) is an ordinary differential equation since the only independent variable is the particle size Dp. For its solution, the required boundary condition is $n^j(0)=0$ (i.e., there are not particles of null size). The analytical solution of

Eq. (8) is given by (Vreman et al., 2009; Bertin et al., 2011)

$$n^j = \frac{1}{G^j} exp\left\{-\frac{1}{G^j}\int_0^{Dp}\frac{1}{\tau^j}\,dDp\right\}\left[\int_0^{Dp}\dot{n}_{in}^j exp\left\{\frac{1}{G^j}\int_0^{Dp}\frac{1}{\tau^j}\,dDp\right\}dDp\right] \tag{9}$$

Even though Eq. (9) is the analytical solution for the PBE, it requires a continuous function to represent the inlet density function flowrate (i.e., seeds PSD), which is instead available as discrete points (experimental data). To this end, the density function flowrate can be also represented in the entire domain of Dp as follows (Hassani, 2009):

$$\dot{n}_{in}^j = \sum_{i=1}^{C}\dot{N}_{i_{in}}^j\,\delta(Dp-\overline{Dp}_i^{m,j}) \tag{10}$$

being C the number of size classes and $\delta(Dp-\overline{Dp}_i^{m,j})$ the Dirac delta function, which has a null value for every size except for $Dp=\overline{Dp}_i^{m,j}$ where its value is infinitely large. $\overline{Dp}_i^{m,j}$ is the appropriate mean diameter in ith class to satisfy the mth moment in jth chamber. The calculation of this mean size is presented later.

Then, by replacing Eq. (10) in (9), the following expression is derived:

$$n^j = \frac{1}{G^j}\sum_{k=1}^{C}\dot{N}_{kin}^j\,exp\left\{-\frac{1}{G^j}\int_{\overline{Dp}_k^{m,j}}^{Dp}\frac{1}{\tau^j}dDp\right\}H(Dp-\overline{Dp}_k^{m,j}) \tag{11}$$

where $H(Dp-\overline{Dp}_k^{m,j})$ is the Heaviside function (Vreman et al., 2009). Eq. (11) is the analytical solution of the steady-state PBE for a perfectly-mixed system where pure coating growth takes place and for an inlet PSD represented by the discrete size distribution given by Eq. (10).

To calculate the particles number within each chamber and class i, Eq. (11) is integrated with respect to Dp between two contiguous nodes as follows:

$$N_i^j = \int_{Dp_i}^{Dp_{i+1}} n^j dDp = \frac{1}{G^j}\sum_{k=1}^{C}\dot{N}_{kin}^j G^j\tau^j \left[e^{-(1/G^j\tau^j)(Dp_i-\overline{Dp}_k^{m,j})H(Dp_i-\overline{Dp}_k^{m,j})} - e^{-(1/G^j\tau^j)(Dp_{i+1}-\overline{Dp}_k^{m,j})H(Dp_{i+1}-\overline{Dp}_k^{m,j})}\right]_{m=0} \tag{12}$$

Therefore, Eq. (12) is the discretized analytical solution in terms of particles number of the steady-state PBE for each perfectly-mixed granulator chamber where pure coating growth is the only mechanism responsible of the particles size changes. Besides, the discrete PSD of the solids leaving chamber j, and expressed in terms of number flowrate, is calculated as $\dot{N}_{iout}^j = N_i^j/\tau^j$.

The particles mass within each chamber j and size class i, m_{Si}^j, is obtained by multiplying Eq. 11 by $\rho_p(\pi/6)Dp^3$ and integrating with respect to Dp between two contiguous nodes

$$m_{Si}^j = \rho_p\frac{\pi}{6}\frac{1}{G^j}\sum_{k=1}^{C}\dot{N}_{kin}^j\int_{Dp_i}^{Dp_{i+1}}Dp^3\,exp\left\{-\frac{Dp-\overline{Dp}_k^{m,j}}{G^j\tau^j}\right\}H(Dp-\overline{Dp}_k^{m,j})dDp \quad m=3 \tag{13}$$

Eq. (13) allows computing exactly the mass within the ith class for any type of grid, avoiding the common problems of different moments closure.

Analogously, the particles surface area for each chamber and class can be calculated by multiplying Eq. (11) by πDp^2 and integrating with respect to Dp between two contiguous nodes:

$$Ap_i^j = \pi\frac{1}{G^j}\sum_{k=1}^{C}\dot{N}_{kin}^j\int_{Dp_i}^{Dp_{i+1}}Dp^2\,exp\left\{-\frac{Dp-\overline{Dp}_k^{m,j}}{G^j\tau^j}\right\}H(Dp-\overline{Dp}_k^{m,j})dDp \quad m=2 \tag{14}$$

Besides providing the PSD of the solids for chamber j, Eqs. (12), (13) and (14) are related to the moments 0, 3 and 2, respectively. In general form, the mth moment is defined as the result of integration of the population number density function over the full

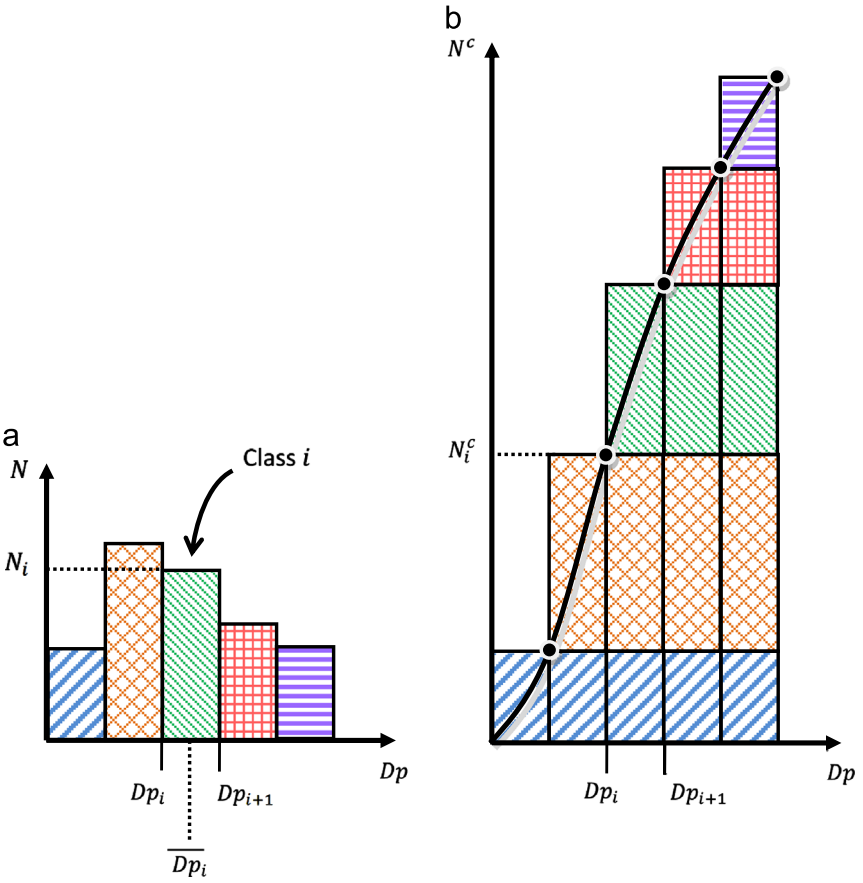

Fig. 3. Histogram (a) and passing cumulative plot (b) for a PSD expressed in terms of particles number.

domain of particles size, weighted with the diameter raised to its *m*th power. Thus, the moments 0, 2 and 3 represent the total number, surface area and mass of particles (Randolph and Larson, 1971). According to the definitions previously described, it is evident that the moments 0, 2 and 3 of the solids within chamber *j*, can also be obtained by adding, respectively, Eqs. , (12), (13) and (14) for all the particle size classes. Fig. 3.

3.1.4. Model solution procedure

To calculate the PSD in each chamber, in terms of particles number by means of Eq. (12) or in terms of particles mass by using Eq. (13), both expressions have to be numerically integrated. For this, G^j and τ^j have to be known. The solution of the mathematical model for each chamber is solved using two iteration loops as indicated in Fig. 4. The internal loop involves the calculation of G^j which, as indicated by Eq. (7), is a function of the total particles surface area; Ap_T^j can be obtained by adding the particles surface area of each class, calculation that requires the knowledge of the PSD within the chambers. Therefore, the PBE in each bed has to be solved iteratively starting with a guess value for G^j . Once the PBE is solved, the total particles surface area can be calculated and then a new value of G^j is computed. This procedure is repeated until convergence. The external loop is required because τ^j depends on the population Sauter diameter, as shown in Fig. 4. The iterative procedure starts by proposing this diameter (see Fig. 4).

The results obtained for the solids stream leaving each chamber are fed to the next one, resulting in a sequential modular model. Fig. 5 shows the procedure to solve the PBE of a given chamber (dotted box in Fig. 4). The PBE solution requires the knowledge of the inlet stream PSD, which is represented as shown in Eq. (10). For chamber 1, the seeds PSD is known and $\overline{Dp}_i^{m,1}$ is assumed to be the mean arithmetic diameter of class *i* for all the moments *m*. Then, the PBE for chamber 1 is solved according to the previously discussed procedure. As a result, the density function within the first granulator compartment is obtained by means of Eq. (11) and, as above mentioned, the discrete values of particles number, mass, surface, etc. per class are determined without discretization errors. For *j* from 2 to 6, if $\dot{N}_{iin}^j$ are assigned to the mean arithmetic diameter of class *i*, the population moment balances will not be perfectly satisfied. To avoid this drawback and minimize the errors propagation along the chambers for the moment *m*, the inlet particles flowrate for the *j*th chamber and *i*th class must be assigned to the mean diameter that conserve the *m*th moment. Thus, the mean diameter $\overline{Dp}_i^{m,j}$ used to calculate the mass per class *i* within chamber *j* by means of Eq. (13) is

$$\overline{Dp}_i^{3,j} = \left(\frac{\dot{m}_{S_{iin}}^j}{\rho_p \dot{N}_{iin}^j(\pi/6)}\right)^{(1/3)} = \left(\frac{\dot{m}_{S_{iout}}^{j-1}}{\rho_p \dot{N}_{iout}^{j-1}(\pi/6)}\right)^{(1/3)} = \left(\frac{m_{S_{iin}}^{j-1}}{\rho_p N_i^{j-1}(\pi/6)}\right)^{(1/3)} \tag{15}$$

Similarly, to calculate the particles surface area for each class and *j* from 2 to 6 that satisfy the total surface area balance, the inlet

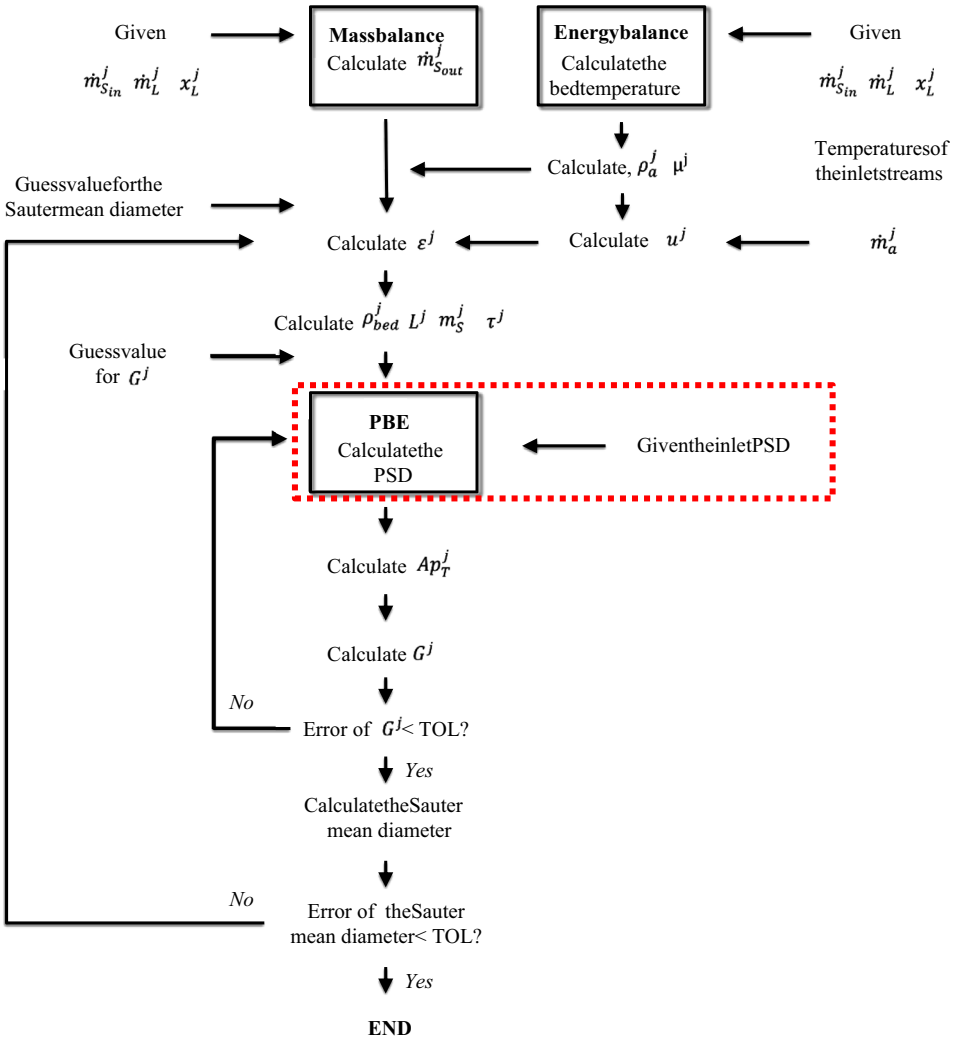

Fig. 4. Solution procedure for the mathematical model of the *j*th chamber.

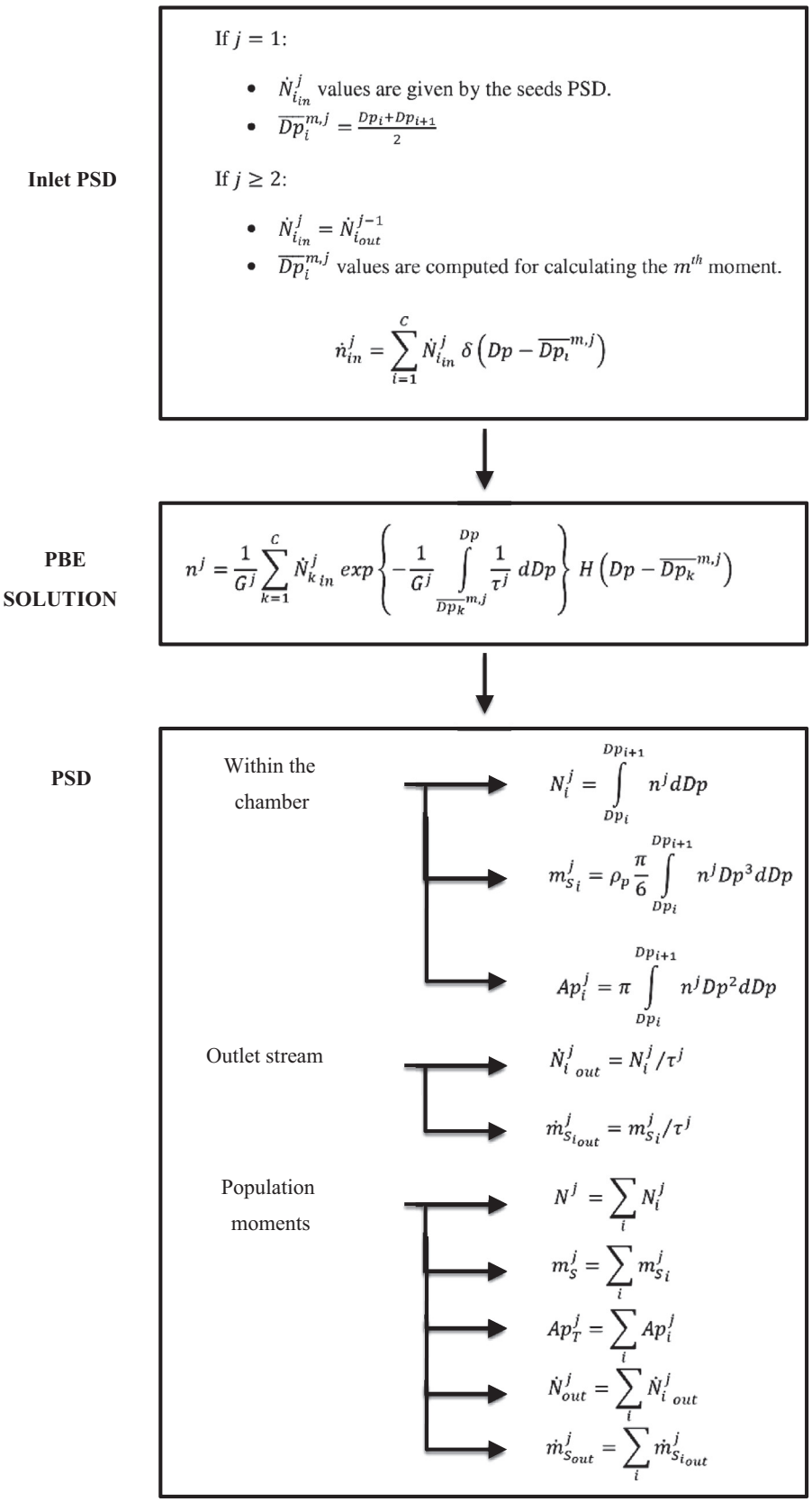

Fig. 5. Procedure to solve the PBE of the *j*th chamber.

particles flowrate for the jth chamber and ith class is assigned to the following mean diameter:

$$\overline{Dp}_i^{2,j} = \left(\frac{Ap_T^{j-1}}{N_i^{j-1}\ \pi} \right)^{(1/3)} \tag{16}$$

The mean diameter given by Eq. (16) is then used to calculate the surface area per class i within chamber j by means of Eq. (14).

3.2. Granulation plant data

To evaluate the goodness of the proposed model to describe the urea granulation process, experimental data from a large-scale multi-chamber fluidized-bed granulator (whose geometric dimensions are available) were used. Samples of the granulator solids inlet and outlet streams were collected every 4 h during 36 h (i.e., 9 data sets) under steady-state operation. For each sampling time, the mass flowrate of the seeds and granulator product were also available (Cotabarren et al., 2009). The urea melt flowrate and water content in the urea solution was obtained from plant online measurements. The sampling of the particulate streams was carried out manually following the guidelines given by Allen (2003). The seeds and granulator product were sampled from the free-falling streams entering and leaving the unit, respectively. The sample cutters were always moved across the entire streams at right angles (i.e., perpendicular to the stream directions), in regular intervals and with relatively constant speed. All the collected samples were placed in labeled sealed bags and reduced to laboratory samples with a chute splitter. The corresponding particle size distributions were determined by the dry sieving method at constant sieving times and agitation rates. A stack of 13 stainless steel sieves and a mechanical sieve shaker were used for the analysis. The standard sieving tower, selected by the industry, consisted of different meshes with apertures varying from 1 to 5 mm.

To compare the PSDs of the seeds and granulator product, the discrete values of the normalized mass density function $\overline{w}_i$ given by Eq. (17) can be used

$$\overline{w}_i = \frac{\overline{W}_i}{Dp_{i+1} - Dp_i} \tag{17}$$

where $\overline{W}_i$ of the class i, corresponding to the range Dp_i–Dp_{i+1}. Fig. 6 presents the normalized mass density functions for the inlet and outlet PSDs.

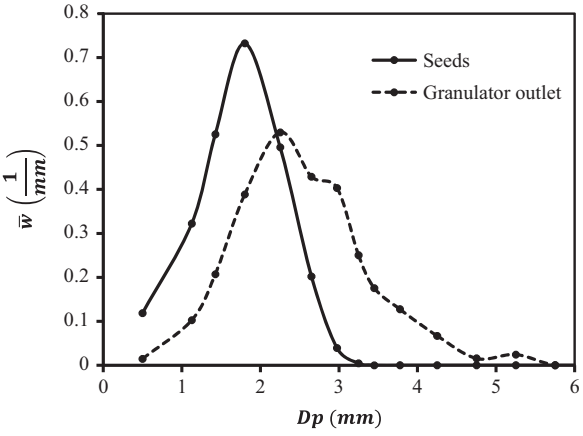

Fig. 6. Experimental normalized mass density functions for given samples of seeds and the granulator outlet stream.

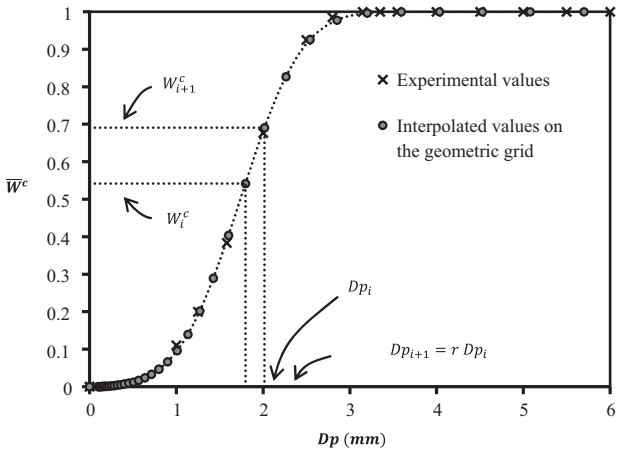

Fig. 7. Passing cumulative distributions for both the experimental and proposed geometric grids.

3.3. Experimental seeds PSDs grid conversion

In order to guarantee the numerical integration accuracy, involved in Eqs. (10) and (13), a reasonable dense grid must be used (Bertin et al., 2011; Qamar and Warnecke, 2007). Consequently, a geometric grid was chosen, being $r=2^{(1/6)}$ the constant ratio between the upper and lower boundaries of any size interval ($r=Dp_{i+1}/Dp_i$). The $2^{(1/6)}$ grid ratio together with the proposed PBE solution method allowed predicting accurately the population moments (e.g., the errors in the predictions of the zero and third moments were lower than 0.001%).

To convert the experimental seeds size distribution (SSD) into the chosen $2^{(1/6)}$ geometric grid, the passing cumulative curve in terms of experimental mass fraction was first constructed. Since the cumulative mass fraction is independent of the grid being used, the cumulative mass fractions for the grid points on the geometric progression higher than 1 mm were calculated by linear interpolation of the available data. Since there was not experimental information for particle sizes smaller than 1 mm, the values of the cumulative curve in the range 0–1 mm were generated using a Rosin–Rammler function (Gupta and Yan, 2006). For the geometric grid, the mass fraction of each size class was easily calculated by means of Eq. (18). Fig. 7 shows the passing cumulative distributions for both the experimental and proposed geometric grids.

$$\overline{W}_i = \overline{W}_{i+1}^c - \overline{W}_i^c \tag{18}$$

Once the mass fraction distributions on the geometric grid were obtained, the PSD was converted to a normalized mass density function by means of Eq. (17).

3.4. Comparison of pure coating growth model predictions with experimental data

In Figs. 8–10, the pure coating growth model predictions (established by using the above proposed model and the corresponding experimental SSD discretized according to the $2^{(1/6)}$ geometric progression) are compared against experimental data, for 3 of the 9 studied cases. As expected, the calculated granules size distributions (CGSD) at the granulator outlet shift towards larger diameters than those of the SSD. Nonetheless, the predicted GSD cannot track the experimental granules size distributions (EGSD) accurately, being the CGSD located on smaller sizes than the EGSD. This behavior was observed for all the analyzed scenarios (i.e., the 9 studied cases). Assuming no significant errors

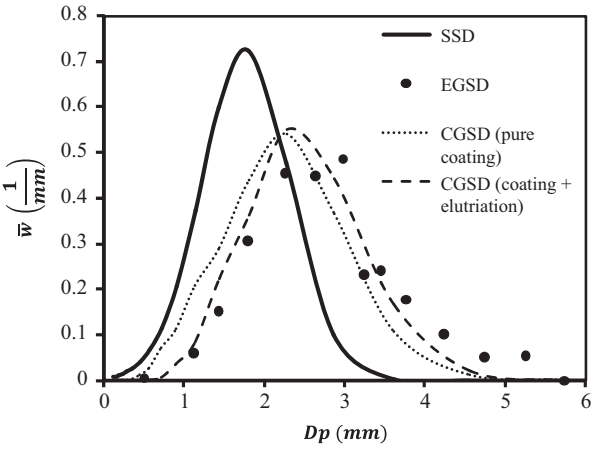

Fig. 8. Comparison of experimental and calculated granules size distributions for case 1 of the 9 studied cases (SSD: experimental seeds size distribution; EGSD: experimental granules size distribution; CGSD: calculated granules size distributions using pure coating and coating and elutriation models).

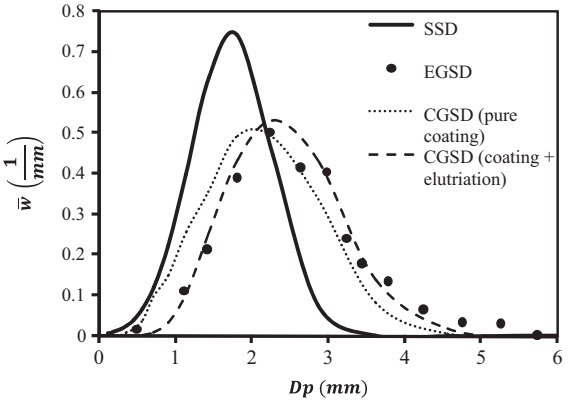

Fig. 9. Comparison of experimental and calculated granules size distributions for case 2 of the 9 studied cases (SSD: experimental seeds size distribution; EGSD: experimental granules size distribution; CGSD: calculated granules size distributions using pure coating and coating and elutriation models).

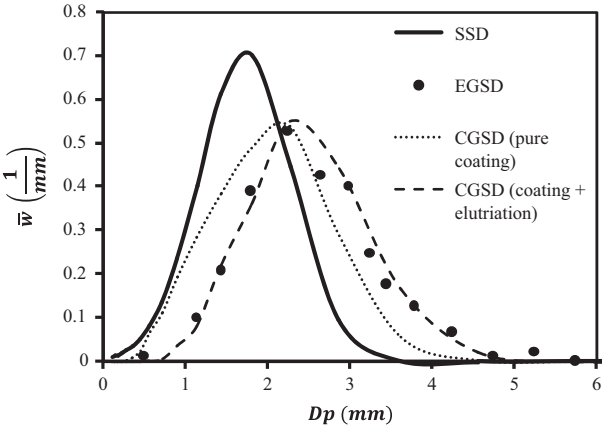

Fig. 10. Comparison of experimental and calculated granules size distributions for case 3 of the 9 studied cases (SSD: experimental seeds size distribution; EGSD: experimental granules size distribution; CGSD: calculated granules size distributions using pure coating and coating and elutriation models).

during samples collection and sieving and considering that the perfectly-mixed configuration is a good representation of the solids flow pattern, the differences found between the model results and the experimental values should be attributed to the presence of an additional mechanism not considered in the previous PBE formulation (Eq. (8)).

Besides coating, other size change mechanisms can shift the PSD towards larger particle diameters, such as the enlargement by agglomeration or fines elutriation. During agglomeration, two or more particles collide and stick together to form new bigger particles (Pietsch, 1991; Ramkrishna, 2000). Agglomeration competes with coating and can become dominant for small particles, high binder flowrates and low fluidization air velocities (Cotabarren et al., 2012). However, experimental evidence indicates that agglomeration is not an important mechanism in the industrial granulator under study and, thus, it can be neglected in the PBE formulation. On the other hand, elutriation is the removal of fines as a consequence of fluidization air velocities higher than the particles terminal velocity (Kunii and Levenspiel, 1991). Elutriation modifies the PSD within the fluidized bed by decreasing the concentration of small particles.

Considering that elutriation is a feasible mechanism within the granulator and that its presence can shift the GSD towards bigger sizes, a new population model was proposed taking into account both the size enlargement by coating and fines elutriation.

4. Fluidized bed granulator model: coating and elutriation

4.1. Mathematical model

The new model was based on the one described in Section 3.1 but reformulating the fourth hypothesis to allow fines elutriation. However, formation of nuclei by attrition, agglomeration, breakage and overspray were still considered negligible. Consequently, the mass balance for each chamber (given by Eq. (1) for pure coating growth) is rewritten as

$$\dot{m}^j_{S_{in}} + \dot{m}^j_L(1-x^j_L) - \dot{m}^j_{S_{out}} - \dot{m}^j_{S_{elu}} = 0 \quad j = 1\text{–}6 \tag{19}$$

where $\dot{m}^j_{S_{elu}}$ is the mass flowrate of particles elutriated from chamber j.

The steady-state PBE for each well-mixed granulator chamber with simultaneous coating and elutriation becomes

$$\frac{d}{dDp}(G^j n^j) = \dot{n}^j_{in} - \frac{n^j}{\tau^j} - \dot{n}^j_{elu} \quad j = 1\text{–}6 \tag{20}$$

where $\dot{n}^j_{elu}$ is the density function flowrate associated to the fines leaving each chamber by elutriation.

According to the approach of Kunii and Levenspiel (1991), the elutriation rate for size class i in each chamber j can be assumed directly proportional to the mass fraction of particles of arithmetic mean size $\overline{Dp}_i$. Therefore, the mass flowrate of elutriated particles belonging to size class i can be written as

$$\dot{m}^j_{i_{elu}} = A^j_T\, k^j_{elu}(\overline{Dp}_i)\overline{W}^j_i \tag{21}$$

where $k^j_{elu}(\overline{Dp}_i)$ is a parameter dependent on the particles size, known as the elutriation rate coefficient. Large values of $k^j_{elu}(\overline{Dp}_i)$ suggest fast removal of size i particles, while $k^j_{elu}(\overline{Dp}_i) = 0$ indicates that the solids belonging to size class i are not removed by elutriation. Eq. (21) can also be expressed in terms of particles number as follows:

$$\dot{N}^j_{ielu} = \frac{A^j_T}{m^j_S}\, k^j_{elu}(\overline{Dp}_i) N^j_i \tag{22}$$

Eqs. (21) and (22) are only valid for those particles with terminal velocities lower than the fluidization air superficial velocity. To include the elutriation mechanism in the PBE, Eq. (21) needs to be rewritten for the entire size domain and in

terms of the number density function

$$\dot{n}^j_{elu} = \frac{A^j_T}{m^j_S} k^j_{elu} \left[1 - H(Dp - Dp^j_{elu})\right] n^j \tag{23}$$

where Dp^j_{elu} is the diameter for which the terminal velocity u^j_t is equal to the superficial velocity u^j. The Heaviside function H assumes a null value for $Dp \le Dp^j_{elu}$, otherwise it is equal to 1. Then Eq. (23) takes nonzero values only for particles with terminal velocities lower than or equal to the fluidization air superficial velocity (i.e., $Dp \le Dp^j_{elu}$), which can be elutriated.

By replacing Eq. (23) in Eq. (20) and considering that G^j is independent of the particle size and that $\dot{n}^j_{out} = n^j/\tau^j$, the steady-state PBE that takes into account both coating and elutriation becomes

$$G^j \frac{dn^j}{dDp} = \dot{n}^j_{in} - \frac{A^j_T}{m^j_S} k^j_{elu} \left[1 - H(Dp - Dp^j_{elu})\right] n^j - \frac{n^j}{\tau^j} \tag{24}$$

There are several correlations to estimate the elutriation rate coefficient k^j_{elu} (Kunii and Levenspiel, 1991). In this work, the following relationship proposed by Colakyan and Levenspiel (1984) was chosen, since it is valid for relatively coarse particles and high fluidization velocities:

$$k^j_{elu} = k_{elu_0}\, \rho_p \left(1 - \frac{u^j_t}{u^j}\right)^2 \tag{25}$$

where k_{elu_0} is the elutriation constant. To determine the value of k_{elu_0} for the large-scale granulator under study, the influence of this parameter on the CGSD was first analyzed. To this end, the particles terminal velocity was calculated for all the size classes and the new PBE model was solved. The following correlation given by Haider and Levenspiel (Kunii and Levenspiel, 1991) was used to calculate the particle terminal velocity:

$$u^j_t = \frac{[(\mu^j(\rho_p - \rho^j_a)g/\rho^{j2}_a)]^{(1/3)}}{(18/Ar^{j(2/3)}) + (0.591/Ar^{j(2/6)})} \tag{26}$$

where μ^j is the air viscosity and Ar^j the Archimedes number (which is a function of the particle size).

The analytical solution of the PBE (Eq. (24)), applying an analogous procedure to the one described for the pure coating model, is given by:

$$n^j = \frac{1}{G^j} \sum_{k=1}^{C} \dot{N}^j_{kin} \exp\left\{ -\frac{1}{G^j} \int_{\overline{Dp}^{m,j}_k}^{Dp} \left[\frac{A^j_T}{m^j_S} k^j_{elu} \left[1 - H(Dp - Dp^j_{elu})\right] + \frac{1}{\tau^j} \right] dDp \right\} H(Dp - \overline{Dp}^{m,j}_k) \tag{27}$$

To calculate the particles number within each chamber j and size class i, Eq. (27) is integrated with respect to Dp between the two contiguous nodes that limit the corresponding size class.

$$N^j_i = \frac{1}{G^j} \sum_{k=1}^{C} \dot{N}^j_{kin} \int_{Dp_i}^{Dp_{i+1}} \exp\left\{ -\frac{1}{G^j} \int_{\overline{Dp}^{m,j}_k}^{Dp} \left[\frac{A^j_T}{m^j_S} k^j_{elu} \left[1 - H(Dp - Dp^j_{elu})\right] + \frac{1}{\tau^j} \right] dDp \right\} H(Dp - \overline{Dp}^{m,j}_k) dDp \tag{28}$$

The particles mass within each chamber j and size class i, m^j_{Si}, is then obtained by multiplying Eq. (27) by $\rho_p(\pi/6)Dp^3$ and integrating with respect to Dp between the two contiguous nodes that limit the size class i

$$m^j_{Si} = \rho_p \frac{\pi}{6} \frac{1}{G^j} \sum_{k=1}^{C} \dot{N}^j_{kin} \int_{Dp_i}^{Dp_{i+1}} Dp^3 \exp\left\{ -\frac{1}{G^j} \int_{\overline{Dp}^{m,j}_k}^{Dp} \left[\frac{A^j_T}{m^j_S} k^j_{elu} \left[1 - H(Dp - Dp^j_{elu})\right] + \frac{1}{\tau^j} \right] dDp \right\} H(Dp - \overline{Dp}^{m,j}_k) dDp \tag{29}$$

Similarly, the particles surface area within each chamber j and size class i, Ap^j_i, is then obtained by multiplying Eq. (27) by $\pi\, Dp^2$ and integrating with respect to Dp between the two contiguous nodes that limit the size class i

$$Ap^j_i = \pi \frac{1}{G^j} \sum_{k=1}^{C} \dot{N}^j_{kin} \int_{Dp_i}^{Dp_{i+1}} Dp^2 \exp\left\{ -\frac{1}{G^j} \int_{\overline{Dp}^{m,j}_k}^{Dp} \left[\frac{A^j_T}{m^j_S} k^j_{elu} \left[1 - H(Dp - Dp^j_{elu})\right] + \frac{1}{\tau^j} \right] dDp \right\} H(Dp - \overline{Dp}^{m,j}_k) dDp \tag{30}$$

The general iterative procedure described in Section 3.1.4 was also applied to solve the granulator model when simultaneous coating and elutriation take place.

4.2. k_{elu_0} fitting from available experimental data

To analyze the influence of the elutriation rate constant on the granulator behavior, the experimental operating conditions corresponding to one of the nine studied cases were selected. For different k_{elu_0} values, Fig. 11 shows the elutriated number fraction (total elutriated number flowrate respect to the seeds one) and the mode of the granulator product PSD expressed in terms of particles number. The reported elutriated fraction corresponds to the total elutriated material that leaves all the chambers. As expected, the elutriated number flowrate increases with k_{elu_0} (see Eq. (22)). For this data set and $k_{elu_0} \ge 0.3$ m/s, the elutriated number fraction is almost constant and close to 55%. For all the tested k_{elu_0}, the elutriated mass flowrate (data not shown) was lower than 0.2% and thus negligible.

As it is shown in Fig. 11 for the selected case, if elutriation is not considered in the model, the number mode of the granular product is around 0.9 mm. On the other hand, when the elutriation mechanism is taken into account in the PBE, the granules number mode increases with k_{elu_0} because more fine particles are removed as the particles population flows through the granulator chambers. In fact, when all the fine particles are elutriated (k_{elu_0} about 0.3 m/s), the granules number mode is close to 1.8 mm.

Once the sensitivity of the model to k_{elu_0} was analyzed, an optimum k_{elu_0} was calculated as the value that minimizes the sum of the squared errors between the measured and predicted GSDs for the nine studied cases. The best k_{elu_0} was found to be approximately 0.15 m/s. This optimum value is one order of magnitude greater than that given by Colakyan and Levenspiel ($k_{elu_0} = 0.011$ m/s). The difference may be attributed to the different dimensions and operating conditions of the fluidized bed investigated in this work and that studied by Colakyan and Levenspiel (1984). Colakyan and Levenspiel (1984) found a value of $k_{elu_0} = 0.011$ m/s for a discontinuous fluidized bed containing particles up to 1 mm and fluidization velocities between 0.9 and 3.7 m/s. In this work, the fluidization air velocities are between 2.5 and 4 m/s while the particles Sauter mean diameter is between 1 and 3 mm.

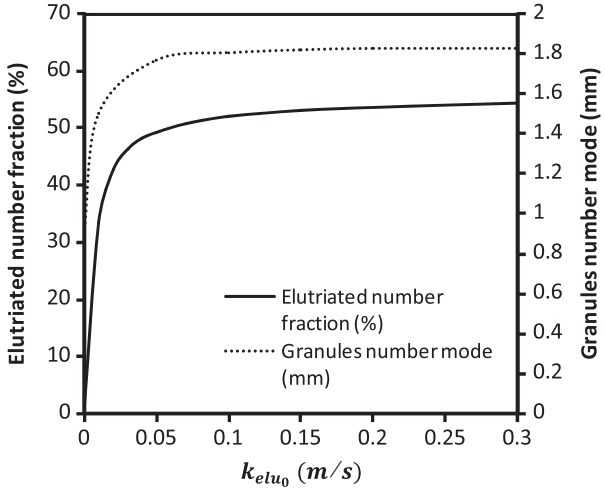

Fig. 11. Elutriated number flowrate (as a fraction of the seeds number flowrate) and mode of the CGSD as a function of k_{elu_0}.

According to the model results obtained for all the studied cases, about 95% and 4% of the particles number are elutriated in the first and second chambers, respectively. Therefore, it can be concluded that for $k_{elu_0}=0.15$ m/s, chamber 3 receives nearly no fines, being the first two fluidized beds responsible for the almost complete elutriation of small particles. Besides, according to the fluidization velocities and the urea and air properties, the critical particle diameter Dp^j_{elu} is found to be approximately 0.6 mm. Therefore, the granulator product PSD has almost no particles with diameters smaller than 0.6 mm.

Figs. 8–10 show, for three of the nine studied cases, the CGSDs by means of the PBE model including coating and elutriation, and using the best-fitting for k_{elu_0}. Regarding the PSDs fine-tail, Figs. 8–10 demonstrate that the model including elutriation gives a better prediction than the one based on just pure coating. Although the model presented in this work showed substantially enhanced performance to predict the granulator product PSD, the tails of coarse particles are still underestimated, suggesting that some other size change mechanism or not perfect coating efficiency might be occurring within the industrial unit. According to experimental data evidence for the 9 studied cases, the agglomeration of particles is not significant. However, it is possible that the amount of agglomerates might be considerable enough to modify the PSD.

In the fertilizers industry, one of the most important parameters to characterize the product quality is the mass median diameter of the product stream that leaves the granulation circuit. Therefore, as an element of a granulation plant simulator, the industrial granulator model must be able to predict the mass median of the population with acceptable accuracy. In this sense, the mass median diameter of the granular product was calculated by means of the pure coating and coating and elutriation models for the nine studied cases. The results indicate that the medians are predicted with errors of 14% and 7% when the pure coating and the coating and elutriation model are used, respectively. Therefore, the median prediction is also substantially improved if elutriation and coating are both considered.

5. Conclusions

For a steady-state perfectly-mixed multichamber granulator and taking into account coating and elutriation, a new PBE solution methodology was proposed to minimize the solution errors propagation expected when a set of PBEs in series is required to be solved. The mass and number population balances (for all the chambers) are closed with very low errors; therefore, the presented solution procedure is superior to other numerical solution techniques that involve the discretization of the particles growth term. Furthermore, the proposed PBE solution method is quite versatile supporting any type of inlet and outlet particle size grids and not necessarily the same ones.

Specifically for the urea granulation case, the fitted granulator model including coating and elutriation considerably improves the prediction of the granules size distribution with respect to the results found when pure coating was assumed. The mathematical representation of the multichamber granulator has a unique fitting parameter: the elutriation constant (k_{elu_0}). For all the studied cases, if k_{elu_0} is higher than 0.15 m/s the model was found to be very insensitive to the elutriation constant value. The results indicate that the fines are removed almost completely in the first and second chambers, being the amount of fines in the subsequent chambers negligible. The influence of elutriation on the particles mass flowrates was not significant; however, the addition of this phenomenon gave a better representation of the number flowrate at the granulator outlet. The median of the GSDs were predicted with average errors lower than 7%. Then, the developed simulation tool constitutes a valuable model to be included as a module of complete granulation plant simulators.

Even though the model presented in this work showed substantially enhanced performance to predict the urea granulator product PSD, the tails of coarse particles are still underestimated. Thus, there is still need to investigate the importance of agglomeration as a particle size change mechanism within the industrial unit. Therefore, the addition of this phenomenon in the population balance equation deserves further research.

Nomenclature

Ap_T	Particles total surface, m^2.
A_0	Passage area, m^2.
Ar	Archimedes number.
A_T	Total cross-sectional area, m^2.
C	Number of classes on a discretized grid.
C_D	Discharge coefficient.
Dp	Particle diameter, m or mm.
$\overline{Dp}$	Particles mean diameter, m or mm.
g	Gravity acceleration, m/s^2.
G	Growth rate, m/s.
H	Heaviside function.
k_{elu}	Elutriation rate coefficient, kg/m^2 s.
k_{elu_0}	Elutriation parameter, m/s.
L	Fluidized-bed height, m.
m_S	Solids mass, kg.
$\dot{m}$	Mass flowrate, kg/s.
$\dot{m}_S$	Solids mass flowrate, kg/s.
n	Number density function, #/mm
$\dot{n}$	Flow of number density function, #/mm s
N	Number, #.
$\dot{N}$	Number flowrate, #/s.
r	Geometric grid ratio between classes.
t	Time, s.
u	Fluidization and atomization air superficial velocity, m/s.
$\dot{W}$	Mass fraction.
$\overline{w}$	Normalized mass density function, 1/mm.
x	Solution water content, wet basis.

Greek letters

δ	Dirac delta function.
ε	Fluidized-bed porosity.
μ	Air viscosity, Pa s.
ρ	Density, kg/m^3.
τ	Quotient between particles mass and particles mass flowrate that leave each chamber, s.

Subscripts

a	Air.
bed	Bed.
elu	Elutriation.
i	Class of the discrete PSD.
in	Inlet.
k	Class of the discrete PSD.
L	Urea solution.
out	Outlet.
p	Particles.
t	Terminal.

Superscripts

c	Cumulative.
j	Chamber.
m	Moment.

References

Adetayo, A.A., 1993. Modelling and Simulation of a Fertilizer Granulation Circuit. University of Queensland, Australia. (Ph.D. thesis).

Adetayo, A.A., Litster, J.D., Cameron, I.T., 1995. Steady state modeling and simulation of a fertilizer granulation circuit. Computers and Chemical Engineering 19 (4), 383–393.

Allen, T., 2003. Powder Sampling and Particle Size Determination. Elsevier, Amsterdam, The Netherlands.

Balliu, N., 2005. An Object Oriented Approach to the Modelling and Dynamics of Granulation Circuits. University of Queensland, Australia. (Ph.D. thesis).

Balliu, N., Cameron, I.T., 2007. Performance assessment and model validation for an industrial granulation circuit. Powder Technology 179 (1–2), 12–24.

Bertin, D.E., Cotabarren, I.M., Bucalá, V., Piña, J, 2011. Analysis of the product granulometry, temperature and mass flow of an industrial multichamber fluidized bed urea granulator. Powder Technology 206, 122–131.

Bertin, D.E., Mazza, G.D., Piña, J., Bucalá, V., 2007. Modeling of an industrial fluidized-bed granulator for urea production. Industrial and Engineering Chemistry Research 46 (23), 7667–7676.

Bertin, D.E., Piña, J., Bucalá, V., 2010. Dynamics of an industrial fluidized bed granulator for urea production. Industrial and Engineering Chemical Research 49 (1), 317–326.

Colakyan, M., Levenspiel, O., 1984. Elutriation from fluidized beds. Powder Technology 38 (3), 223–232.

Cotabarren, I., Bertin, D., Piña, J., Bucalá, V., Romagnoli, J., 2009. Dynamic simulation and optimization of a urea granulation circuit. Chemical Engineering Transactions 17, 723–728.

Cotabarren, I.M., Bertin, D., Piña, J., Bucalá, V., 2011. Analysis of optimal control problems and plant debottlenecking for urea granulation circuits. Industrial and Engineering Chemistry Research 50, 11996–12010. (ISSN 0888-5885).

Cotabarren, I.M., Bertin, D.E., Veliz Moraga, S., Mirazú, L., Piña, J., Bucalá, V., 2012. Production of granular urea as nitrogenous fertilizerUrea: Synthesis, Properties and Uses. NOVA Science Publishers, New York.

Dosta, M., Heinrich, S., Werther, J., 2010. "Fluidized bed spray granulation: Analysis of the system behaviour by means of dynamic flowsheet simulation". Powder Technology 204 (1), 71–82.

Ennis, B.J., 1997. In: Behringer, R.P., Jenkins, J.T. (Eds.), "Unto dust shalt thou return", in Powders and Grains, 97. A.A. Balkema, Rotterdam, pp. 13–23.

Gatzke, E., Doyle III, F.J., 2001. Model predictive control of a granulation system using soft output constraints and prioritized control objectives. Powder Technology 121, 149–158.

Grieco, E., Marmo, L., 2006. Predicting the pressure drop across the solids flow rate control device of a circulating fluidized bed. Powder Technology 161, 89–97.

Gupta, A., Yan, D., 2006. Mineral Processing Design and Operation, an Introduction. Elsevier, Amsterdam, The Netherlands.

Hassani, S., 2009. Mathematical Methods for Students of Physics and Related Fields. Springer, New York. (ISBN: 978-0-387-09503-5).

Kayaert, A.F., Antonus, R.A.C., 1997. Process for the Production of Urea Granules. US Patent 5653781.

Kunii, D., Levenspiel, O., 1991. Fluidization Engineering. Butterworth-Heinemann, Newton.

Litster, J., Ennis, B., Liu, L, 2004. The science and engineering of granulation processesParticle Technology SeriesKluwer Academic Publishers, Dordrecht.

Massimilla, L., 1971. Flow properties of the fluidized dense phase". In: Davidson, J.F., Harrison, D. (Eds.), Fluidization. Academic Press, New York.

Massimilla, L., Betta, V., Della Rocca, C., 1961. A study of streams of solids flowing from solid-gas fluidized beds. AIChE Journal 7, 502–508.

Mörl, L., Heinrich, S., Peglow, M., 2007. Fluidized bed spray granulation. In: Salman, A.D., Hounslow, M.J., Seville, J.P.K (Eds.), Handbook of Powder Technology. Elsevier, Amsterdam, The Netherlands.

Niks, A., Van Hijfte, W.H.P., Goethals, R.A.J., 1980. Process for Urea Granulation. U.S. Patent 4219589.

Pietsch, W., 1991. Size Enlargement by Agglomeration. John Wiley & Sons Ltd., Chichester, England.

Qamar, S., Warnecke, G., 2007. "Numerical solution of population balance equations for nucleation, growth and aggregation processes". Computers and Chemical Engineering 31 (12), 1576–1589.

Radichkov, R., Müller, T., Kienle, A., Heinrich, S., Peglow, M., Mörl, L., 2006. A numerical bifurcation analysis of continuous fluidized bed spray granulation with external product classification. Chemical Engineering and Processing 45 (10), 826–837.

Ramkrishna, D., 2000. Population Balances. Academic Press, London, England.

Randolph, A.D., Larson, M.A., 1971. Theory of Particulate Processes. Academic Press, New York, USA.

Reimers, C., Werther, J., Gruhn, G., 2009. Design specifications in the flowsheet simulation of complex solids processes. Powder Technology 191 (3), 260–271.

Richardson, J.F., Zaki, W.N., 1954. Sedimentation and fluidization, part I, transactions of the institution of chemical engineers. Institute of Chemical Engineering 32, 35–53.

Sanders, C.F.W., Hounslow, M.J., Doyle III, F.J., 2009. Identification of models for control of wet granulation. Powder Technology 188, 255–263.

Tan, H.S., Salman, A.D., Hounslow, M.J., 2006. Kinetics of fluidised bed melt granulation I, the effect of process variables. Chemical Engineering Science 6, 1585–1601.

Vreman, A.W., van Lare, C.E., Hounslow, M.J., 2009. A basic population balance model for fluid bed spray granulation. Chemical Engineering Science 64, 4389–4398.

Wang, F.Y., Cameron, I.T., 2007. A multi-form modelling approach to the dynamics and control of drum granulation processes. Powder Technology 179 (1–2), 2–11.

Werther, J., Heinrich, S., Dosta, M., Hartge, E.-U., 2011. The ultimate goal of modeling – simulation of system and plant performance. Particuology 9 (4), 320–329.

Wildeboer, W.J., 1998. Steady State and Dynamic Simulations of a Closed Loop Granulation Circuit. Delft University of Technology, The Netherlands. (Master thesis).